

# Geometrical, electronic and magnetic properties of $\text{Na}_{0.5}\text{CoO}_2$ from first principles

Zhenyu Li, Jinlong Yang,\* J.G. Hou, and Qingshi Zhu  
*Hefei National Laboratory for Physical Sciences at Microscale,  
Laboratory of Bond Selective Chemistry,  
and Structure Research Laboratory,  
University of Science and Technology of China, Hefei, Anhui 230026, P.R. China*

(Dated: November 20, 2018)

## Abstract

We report a first-principles projector augmented wave (PAW) study on  $\text{Na}_{0.5}\text{CoO}_2$ . With the sodium ion ordered insulating phase being identified in experiments, pure density functional calculations fail to predict an insulating ground state, which indicates that Na ordering alone can not produce accompanying Co charge ordering, if additional correlation is not properly considered. At this level of theory, the most stable phase presents ferromagnetic ordering within the  $\text{CoO}_2$  layer and antiferromagnetic coupling between these layers. When the on-site Coulomb interaction for Co  $3d$  orbitals is included by an additional Hubbard parameter  $U$ , charge ordered insulating ground state can be obtained. The effect of on-site interaction magnitude on electronic structure is studied. At a moderate value of  $U$  (4.0 eV for example), the ground state is antiferromagnetic, with a  $\text{Co}^{4+}$  magnetic moment about  $1.0 \mu_B$  and a magnetic energy of 0.12 eV/Co. The rehybridization process is also studied in the DFT+U point of view.

PACS numbers: 71.28.+d, 71.27.+a, 75.25.+z

## I. INTRODUCTION

$\text{Na}_x\text{CoO}_2$  was originally studied as a kind of rechargeable battery material<sup>1</sup> and thermoelectric material<sup>2,3,4</sup>. More recently, the discovery of the superconductivity in its hydrated  $x=0.35$  compound<sup>5</sup>, where the effect of hydration is found to be limited to lattice expansion<sup>6,7</sup>, makes it receive a renewed interest.  $\text{Na}_x\text{CoO}_2$  has a crystal structure consisting of 2D triangular lattice Co sheets, octahedrally coordinated with O above and below the Co planes, and layers of Na ions sandwiched between the  $\text{CoO}_2$  sheets. The phase diagram of  $\text{Na}_x\text{CoO}_2$  has been determined by changing the Na content  $x$  using a series of chemical reactions<sup>8</sup>. Their electronic and magnetic properties are found to be strongly dependent on the number of charge carriers introduced by deviations from stoichiometry in the Na sublattice.

Theoretical studies on the electronic structure of  $\text{Na}_x\text{CoO}_2$  are very active. The early work by Singh<sup>9,10</sup> focused on the magnetic properties. He predicted a weak instabilities of itinerant ferromagnetic character in range  $x = 0.3$  to  $x = 0.7$ , with competing but weaker itinerant antiferromagnetic solution. He used the virtual crystal approximation, instead of supercell model, to describe the partially occupation of Na sites. As a result, the possibility of sodium ion and  $\text{Co}^{3+}/\text{Co}^{4+}$  charge ordering is not allowed. Using pseudopotential plane wave method, Ni *et al.*<sup>11</sup> have optimized the geometries for  $\text{Na}_x\text{CoO}_2$  ( $x = 0.25, 0.5, 0.75$  and  $x = 1$ ) with a  $2 \times 2 \times 1$  supercell. They found that the itinerant ferromagnetism is strongly suppressed by the local distortions of the oxygen around the cobalt. With optimized geometries, they identified a phase transition from wide-band ferromagnetic to narrow band paramagnetic metals with  $x$  increasing. By carefully examining the doped electron density, Marianetti *et al.*<sup>6</sup> found that the rigid band model is not suitable for this Na doped system. A rehybridization driven by a competition between the on-site Coulomb interaction and the  $e_g$ -oxygen hybridization is identified. They have also used a modified Hubbard model to study this kind of rehybridization. Within the framework of density functional theory (DFT), the on-site Coulomb correlation effects can be dealt with DFT+U method<sup>12</sup>. Using this method, Zou *et al.*<sup>13</sup> have studied the electronic structure of  $\text{Na}_x\text{CoO}_2$  with varying  $c/a$  ratio. They did not find critical change of the band structure near  $E_F$ , except a notable decrease of the DOS at  $E_F$ . To consider the relations between correlation and charge ordering, Pickett and coauthors<sup>14,15</sup> have applied the DFT+U method to a  $\sqrt{3} \times \sqrt{3} \times \frac{1}{2}$  supercell of  $\text{Na}_x\text{CoO}_2$

at  $x = 1/3$  and  $x = 2/3$ . They found that the parameter  $U$  is critical to charge and spin orderings (for small supercell, the so called charge disproportionation always leads to charge ordering). They suggested that the phase diagram of  $\text{Na}_x\text{CoO}_2$  is characterized by a crossover from effective single-band character with  $U \gg W$  for  $x > 0.5$  into a three-band regime for  $x < 0.5$ , where  $U \sim W$  and correlation effects are substantially reduced.

$\text{Na}_{0.5}\text{CoO}_2$  is of special interests among the  $\text{Na}_x\text{CoO}_2$  family. In the recent experimental phase diagram of  $\text{Na}_x\text{CoO}_2$ , a novel sodium ion ordered insulating state at  $x = 0.5$  was found<sup>8</sup>, with the most strongly developed superstructure<sup>16,17</sup>. This insulating state separates two kinds of metallic phase, *i.e.* Curie-Weiss metal for  $x > 0.5$  and paramagnetic metal for  $x < 0.5$ . It is suggested that the occurrence of the insulating state indicates a strong interaction between the ions and holes even though they occupy separate layers, and a charge ordering is thought to accompany the sodium ion ordering<sup>8</sup>. Therefore it is interesting to compare the electronic structure based on this experimental sodium ion ordered structure with previous theoretical results to identify the effect of Na ordering. For example, it will be interesting to see if the Na ordering will produce a Co charge ordering at DFT level. On the other hand, the correlation effects of  $\text{Na}_{0.5}\text{CoO}_2$  is considered to be a betweenness comparing to small values for  $x > 0.5$  and relatively large values for  $x < 0.5$ <sup>11,15</sup>, which demands a study at the DFT+U level to identify the effect of correlation. Unfortunately, there is no theoretical work in the literature for this important  $x = 0.5$  case with both Na ordering and correlation effects being properly considered. In this paper, we report the electronic structure of  $\text{Na}_{0.5}\text{CoO}_2$  focusing on the possibility of charge ordering and based on the experimental superstructure at both DFT and DFT+U level.

## II. COMPUTATIONAL METHOD

The calculations in this work were performed with the Vienna *Ab initio* Simulation Package (VASP)<sup>18,19</sup>, which is a first-principles plane-wave code, treating the exchange and correlation in the DFT scheme. In this study, the Perdew-Wang functional form<sup>20</sup> of generalized gradient approximation (GGA) was used. For spin-polarized calculations, the spin interpolation of Vosko *et al.*<sup>21</sup> was also adopted. The projector augmented wave (PAW)<sup>22</sup> method in its implementation of Kresse and Joubert<sup>23</sup> was used to describe the electron-ion interaction. The Kohn-Sham equations were solved via a Davidson-block iteration scheme<sup>18</sup>.

A  $\sqrt{3} \times 2 \times 1$  supercell was introduced to describe the experimental sodium ion ordering. Brillouin zone (BZ) integrations were performed on a well converged grid of  $8 \times 8 \times 4$  Monkhorst-Pack<sup>24</sup> special points. The total energy and density of states (DOS) were calculated using the linear tetrahedron method with Blochl corrections<sup>25</sup>. The plane wave kinetic energy cutoff was fixed to 500 eV. Dudarev *et al.*'s approach<sup>26</sup> was adopted for DFT+U calculations. Since this DFT+U functional depends only on the difference of Hubbard parameter  $U$  and screened exchange parameter  $J$ ,  $J$  was fixed to 1 eV during all DFT+U calculations. The Hubbard on-site Coulomb interaction is applied to Co  $3d$  orbitals only. Geometry relaxation is performed at a spin unpolarized GGA level.

### III. RESULTS AND DISCUSSION

#### A. Geometrical properties

A  $\sqrt{3} \times 2 \times 1$  superstructure of  $\text{Na}_{0.5}\text{CoO}_2$  has been found by powder neutron diffraction experiment<sup>16</sup>. This superstructure has the  $Pnmm$  space group symmetry, with a cell formula:  $\text{Na}_4\text{Co}_8\text{O}_{16}$ . In this experimental structure model, the Na1 and Na2 sites ( $2b$  and  $2d$  Wyckoff sites for original  $P6_3/mmc$  space group, and  $2b$  and  $2a$  sites for this  $Pnmm$  space group respectively) are equally occupied, and the ordered Na ions form one-dimensional zigzag chains. Two types of Co ions ( $4f$  and  $4d$ ), which differ subtly in their coordination by oxygen, are also in chains. The existence of two kinds of Co sites allows the emergence of two inequivalent Co ions, namely  $\text{Co}^{3+}$  and  $\text{Co}^{4+}$ , in the process of self-consistency. Therefore this structure model can be used to study the possibility of charge ordering.

The geometry optimization, starting from the experimental structure, reaches its convergence until all forces vanished within 0.01 eV/Å. The optimized geometry is shown in Fig. 1. During the optimization, the cell parameters are fixed to the experimental values ( $a = 4.876$  Å,  $b = 5.630$  Å, and  $c = 11.063$  Å), which results in only a neglectable stress less than 20 kB. As listed in Table I, relaxations of atomic positions from the experimental ones are also found to be very small. The largest relaxation comes from the first two Na atoms along  $x$  direction (0.06 Å), typical relaxations are about 0.01~0.02 Å. The calculated two kinds of Co-O distances (1.91 Å and 1.88 Å) are very similar to experimental values (1.90 Å and 1.86 Å). In an ideal structure model of  $\text{Na}_x\text{CoO}_2$ , Co and O may form layers of

edge-shared  $\text{CoO}_6$  octahedra in a triangular lattice, but distortion of the octahedra with the variation of the O height  $z_0$  from its ideal value is always exists in real system. Our optimized  $z_0$  varies from  $0.0845 c$  to  $0.0892 c$  for different O sites, resulting in the Co-O-Co angles varying from  $96.2^\circ$  to  $97.0^\circ$ . Comparing to the  $90^\circ$  angle in the undistorted octahedra, the optimized structure shows a considerable distortion of the oxygen octahedra. For  $2 \times 2 \times 1$  supercell, we get a slightly smaller distortion, but Ni *et al.*<sup>11</sup> get a significantly larger one. We notice that they have used a relatively small kinetic energy cutoff in their study.

## B. GGA electronic structure

We can clearly identify three well separated manifolds in the paramagnetic GGA band structure and DOS of  $\text{Na}_{0.5}\text{CoO}_2$ , as shown in Fig. 2. The lowest in energy is the O  $2p$  bands, with a bandwidth about 5.5 eV (only part of them are shown in the figure). The other two manifolds come from the Co  $3d$  orbitals, which are splitted into a lower lying  $t_{2g}$  manifold and an upper lying  $e_g$  manifold, separated by approximately 2.5 eV according to the oxygen octahedral crystal field. Although these three manifolds are well separated in energy, the hybridizations of O  $2p$  states with both the  $t_{2g}$  and  $e_g$  states are notable. The Fermi energy locates at the upper edge of the  $t_{2g}$  manifold, indicating a metallic GGA ground state.

The low energy properties of  $\text{Na}_{0.5}\text{CoO}_2$  will be determined by the  $t_{2g}$  manifold, which has a bandwidth of 1.6 eV. The trigonal symmetry of the Co sites further splits the  $t_{2g}$  states into one with  $a_g$  symmetry and a doubly degenerate  $e'_g$  pair. In Fig. 2, we also plot the  $a_g$  (Co  $d_{z^2}$ ) partial DOS. As found by Lee *et al.*<sup>15</sup>, the  $a_g$  states have a bandwidth almost identical to that of the whole  $t_{2g}$  manifold, which indicates that the widely used single-band model may not be sufficient enough to describe the GGA electronic structure of this material.

Fermi surface often plays an important role in the electronic structure of materials. Our GGA Fermi surfaces for the five bands across Fermi level are shown in Fig. 3, which are obtained by a  $32 \times 28 \times 14$  BZ sampling and viewed by XCrySDeN package<sup>27</sup>. LDA/GGA band structure is expected to give valuable and accurate information about the Fermi surface even in system with strong correlations<sup>7</sup>. In our supercell structure, there will be band folding from the first BZ of the original hexagonal lattice (black hexagon in the Fig. 3a), and the

Fermi surface thus becomes very complex. We notice that, on the other hand, the band structure of the superstructure geometry is far from simply band folding, for example, the Fermi surface of the fourth band (band 99) shows a prominent 3D character, which has not been reported in previous virtual crystal study<sup>9,10</sup>. According to the complexity of the present Fermi surfaces, nesting effect for  $\text{Na}_{0.5}\text{CoO}_2$  may not be very strong, and we thus don't expect to find corresponding spin density wave (SDW) state.

Spin-polarized calculations are carried out in order to address the possibility of magnetic ordering. When the ordering is constrained to be ferromagnetic (FM), a stable low spin solution is obtained, with magnetic moments of 0.4 and 0.45  $\mu_B$  for Co1 and Co2 respectively. But the corresponding energy gain from ferromagnetic instability is only 26 meV/Co. The moment values are somewhat smaller than that (0.5  $\mu_B$ ) reported by Singh<sup>9</sup> under virtual crystal approximation, which may due to the difference between their structural model and ours. In our structure, the triangular symmetry is slightly broken.

Antiferromagnetic (AFM) ordering is frustrated on the 2D triangular lattice. But if the magnetic moments on a sublattice vanish, the left other sublattice may geometrically permit the presence of AFM ordering. Here we get an AFM model (AFM1) by fixing the magnetic moments at Co1 sites to be zero. As shown in Fig. 1, the Co2 sites form a 1D chain in the  $x$ - $y$  plane, and it is easy to establish AFM ordering within this chain. In a unit cell, the two AFM chains are set to be out of phase. The AFM1 model results in a magnetic moments of Co2 ions about 0.39  $\mu_B$ , which is much larger the result (0.21  $\mu_B$ ) for the Singh's AFM model<sup>9</sup>. We notice that in that model each Co ion has also two nearest neighbors of like spin in addition to four of opposite spin. Another AFM model (AFM2) is constructed by alter the direction of magnetic moments of neighboring FM Co layers. Although the interlayer exchange interaction is expected to be small, we get lower energy for AFM2 state than that of FM state.

Until now, we get a metallic ground state with intra-layer FM ordering and inter-layer AFM ordering. Comparing with the results of Singh<sup>9</sup>, we may conclude that Na ordering alone will not qualitatively affect the GGA electronic structure to generate the band gap and charge ordering observed in experiments. For the AFM1 state, where charge ordering is enforced, the magnetic energy (7 meV/Co) is much smaller than those of AFM2 and FM states, which indicates the enforced charge ordering under GGA level is unfavorable in energy. This result is consistent with the calculations for  $\text{Na}_{1/3}\text{CoO}_2$ , where attempts using

LDA to obtain self-consistent AFM spin ordering always converge to the FM or nonmagnetic solution<sup>14</sup>. This discrepancy between theory and experimental observation naturally leads to a further consideration of correlation effect.

### C. DFT+U electronic structure

DFT+U<sup>12,26</sup> is a kind of method aiming to deal with the on-site Coulomb interaction within the framework of DFT. It treats the local electrons in a Hartree-Fock manner, which drives local orbital occupations to integral occupancy as  $U$  increases. For transition metal oxide, one may find a larger split of  $d$  orbitals for larger  $U$ , as shown in Fig. 4-6, where partial DOS of cobalt  $3d$  orbitals and oxygen  $2p$  orbitals are plotted for FM, AFM1 and AFM2 states respectively. The cobalt  $3d$  partial DOS for Co1 and Co2 sites are separated. We do not present the results for spin restricted paramagnetic states in this section, because the energy differences between these states and corresponding magnetic states increase rapidly with  $U$  (0.4 eV/Co for  $U = 7.0$  eV). The paramagnetic states are still metallic even with  $U$  as large as 7.0 eV.

In Fig. 4, the top panel is the GGA result, and the three below panels represent three typical electronic structure behaviors for different  $U$  values. For small  $U$  (see panel b), the electronic structure is similar to the above GGA one, except for a strong trend towards gap opening and charge ordering. As shown in Fig. 7, the moments on the two inequivalent Co sites are nearly equal and also similar to the GGA values (which is the  $(U - J) \rightarrow 0$  limit) until  $U = U_c = 3$  eV. Above  $U_c$ , the unoccupied part of the  $a_g$  states weight more and more for Co2 states with the increase of  $U$ . Disproportionation from  $\text{Co}^{3.5+}$  into  $s = \frac{1}{2}$   $\text{Co}^{4+}$  and  $s = 0$   $\text{Co}^{3+}$  ions is nearly complete at  $U = 4$  eV and is accompanied by a metal insulator (Mott-like) transition from conducting to insulating. This insulating phase results from the splitting of the  $a_g$  states, which lead to an unoccupied narrow band containing one hole for each Co2 ions and an occupied band on the Co1 ion, as shown in Fig. 4c. We judge the formation of charge ordering from local magnetic moments instead of from charge population directly, because the charge difference between Co1 and Co2 are relatively small (only 0.1~0.2 electron). This is a result of the hybridization of the O  $2p$  and Co  $3d$  orbitals. In fact, oxygen may directly contribute to the charge ordering in some oxides, as suggested by Coey<sup>28</sup>. We also notice that the charge ordering and gap opening with a moderate  $U$  is

far from obvious, since Zou *et al.*<sup>13</sup> have gotten a metallic ground state with a relatively large Coulomb  $U$  (5 eV) but without adopting any supercell structure. Therefore the sodium ion ordering is critical to the insulating ground state.

There is no clear boundary for moderate and large values of  $U$ , but a relatively large  $U$  value will feature several characters as shown in Fig. 4d. First, the empty  $a_g$  bands are pushed further higher, which makes them strongly mix with the upper  $e_g$  bands. Secondly, the large splitting of the Co  $3d$  orbitals even squeeze some Co  $2 3d$  states to the bottom of the O  $2p$  manifold, and consequently the O  $2p$  character at the edge of the valence band near Fermi energy has exceeded the Co  $3d$  characters. Thirdly, the magnetic moments of cobalt are exceeded  $1 \mu_B$  in this region (up to  $1.42 \mu_B$  per Co for  $U = 7.0$  eV), which seems curious at first sight. We now give two possible rationalizations for this observation. One interpretation comes from the population analysis process. We notice that oxygen is also spin polarized in our calculations for large  $U$ , which makes the net magnetic moment of the whole supercell still about  $1.0 \mu_B$  per Co. Therefore the nominal magnetic moment being larger than  $1 \mu_B$  per Co may be just an artifact of PAW population analysis as a result of the strong hybridization between Co and O. Another possibility is that the large on-site Coulomb interaction may really promote a transition from low spin state to an intermediate spin state as demonstrated by Korotin *et al.*<sup>29</sup> for Co ions in vertex sharing  $\text{CoO}_6$  octahedra. This type of transition is consistent with the strong mixing of empty  $a_g$  and  $e_g$  bands.

The evolution of electronic structures with  $U$  for AFM states is generally similar to that for FM state. The most significant difference is that the charge ordering occurs well before gap opening for AFM1 state. As shown in Fig. 7, the  $\text{Co}^{4+}$  moment grows immediately for AFM1 state as  $U$  increases from 1 eV, but the gap opens until  $U = 3$  eV, which is different from the results of Lee *et al.*<sup>15</sup> for  $\text{Na}_x\text{CoO}_2$  with  $x = 1/3$  and  $x = 2/3$ .

The energy difference between the FM and AFM phases as a function of  $U$  is plotted in Fig. 7c. The general trend gives lower energy AFM state for small  $U$  and lower energy FM state for large  $U$ , except the relatively higher AFM1 energy for small  $U$ , which is caused by the artificial charge ordering as previously discussed. For large  $U$ , the lower energy of FM state is a natural result of the weakening of superexchange effect, and it is also consistent with the prominent DOS of the majority spin component at deep energy as shown in Fig. 4d. The energy difference between FM and AFM2 is generally small according to the relatively small exchange interaction between different layers. According to our result, the magnitude



of on-site Coulomb interaction  $U$  in this material can be probed by experimental magnetic measurement.

From Fig. 4-6, we can find an interesting splitting and ordering of the  $e_g$  orbitals. With the increase of  $U$ , the lower part of the  $e_g$  orbitals becomes mainly from Co1 sites and the upper part from Co2 sites. We notice that this kind of orbital ordering of unoccupied  $e_g$  orbitals will not affect the low energy properties of  $\text{Na}_{0.5}\text{CoO}_2$ . Although it has been found in  $\text{LaCoO}_3$ <sup>29</sup>, orbital ordering of valence band orbitals is not very possible in this structure, since they are not doubly degenerated.

A rehybridization process is proposed to describe the competition between the on-site Coulomb interaction and the  $e_g$ -oxygen hybridization in doped CoO layers<sup>6</sup>. This process can be seen clearly from the partial DOS of O  $2p$  orbitals as shown in Fig. 4-6. At GGA level, hybridization of oxygen  $2p$  states and  $e_g$  states are more significant than the  $t_{2g}$ -oxygen hybridization. With the increase of  $U$ , the on-site Coulomb interaction becomes stronger, which can be minimized by unmixing the oxygen and  $e_g$  orbitals in order to decrease the occupation of the  $e_g$  orbitals. In Fig. 4-6, we can clearly see this kind of unmixing by the decrease of oxygen  $2p$  partial DOS in the  $e_g$  manifold. For large value of  $U$ , the hybridization of oxygen  $2p$  states and  $t_{2g}$  states is somewhat enhanced, which is not included in the modified Hubbard model study by Marianetti *et al.*<sup>6</sup>.

We have studied the effect of Hubbard  $U$  on the electronic structures of  $\text{Na}_{0.5}\text{CoO}_2$  in the previous part of this section, but the actual value of  $U$  in this material is not determined yet, of which very different values are proposed in the literature<sup>9,13,15,32</sup>. Based on the following two experimental observes, we estimate that the value of  $U$  should be moderate, as also suggested by Lee *et al.*<sup>15</sup>. First, the insulating ground state suggests that the value of  $U$  should not be too small. Secondly,  $\text{Na}_x\text{CoO}_2$  with  $x$  away from 0.5 is always metallic indicates a narrow energy gap for  $\text{Na}_{0.5}\text{CoO}_2$ , which prefer a not too large value of  $U$ . Since there was experimental report<sup>33</sup> on electron mass enhancement for small  $x$  of  $\text{Na}_x\text{CoO}_2$ , people have compared the experimental electronic specific heat coefficient  $\gamma$  with the band value to estimate the strength of correlation<sup>9,15</sup>. But in the  $\text{Na}_{0.5}\text{CoO}_2$  case, where Hubbard type correlation drives system to a Mott insulator,  $\gamma$  will reduced by the correlation effects. In fact, the experimental  $\gamma$  is only 3 mJ/mol-K<sup>2</sup>,<sup>16</sup> which is much smaller than our GGA band value (10.5 mJ/mol-K<sup>2</sup>), but very near to the DFT+U value (zero).

At a plausible value of  $U$ , 4 eV for example, intralayer AFM coupling is favored over

FM and interlayer AFM coupling (ref Fig. 7c). We notice that the magnetic state in  $\text{Na}_x\text{CoO}_2$  is far from being clearly determined in experiments. There are some experiments supporting AFM coupling<sup>30,31</sup>, while there are also some recent experiments supporting FM coupling<sup>30,34,35</sup>. With this intermediate value of  $U$ , the ground state (AFM1) magnetic moment for  $\text{Co}_2$  is  $1.0 \mu_B$ , and the magnetic energy is  $0.123 \text{ eV/Co}$ .

#### IV. CONCLUSION

Based on DFT+U method, we have studied the effects of Na ordering and on-site Coulomb correlation on the geometrical, electronic and magnetic properties of  $\text{Na}_{0.5}\text{CoO}_2$ . Without including on-site Coulomb interaction  $U$ , the experimental insulating phase can not be produced by DFT. For small value of  $U$ , ground state is still metallic. At this time, no charge ordering occur for FM coupling, and symmetry enforced charge ordering for intralayer AFM coupling is unfavorable in energy. Increasing parameter  $U$  to a moderate value can open an energy gap and form charge ordering for both FM and AFM states. Large  $U$  value will largely split the Co  $3d$  orbitals, which leads to squeezing Co  $3d$  states to the bottom of O  $2p$  manifold, mixing of empty  $a_g$  and  $e_g$  states, and large Co magnetic moments.

Accompanying with the early work on  $\text{Na}_x\text{CoO}_2$  ( $x = 1/3$  and  $x = 2/3$ )<sup>14,15</sup>, our study will shed some insights into understanding of the complex interplay of Na content, superstructure, correlation effects and tendency of various type of ordering in  $\text{Na}_x\text{CoO}_2$ . However, a complete understanding on this issue, for example, why the  $x = 2/3$  case with stronger commensurability effect and maybe also stronger correlation is not a charge ordered insulator in experiment, will need much further work.

#### Acknowledgments

This work is partially supported by the National Project for the Development of Key Fundamental Sciences in China (G1999075305, G2001CB3095), by the National Natural Science Foundation of China (50121202, 20025309, 10074058), by the Foundation of Ministry

of Education of China, and by ICTS, CAS.

---

- \* Corresponding author. E-mail: jlyang@ustc.edu.cn
- <sup>1</sup> C. Fouassier, C. Delmas, and P. Hagemuller, *Mater. Res. Bull.* **10**, 443 (1975)
- <sup>2</sup> I. Terasaki, Y. Sasago, and K. Uchinokura, *Phys. Rev. B* **56**, 12685 (1997)
- <sup>3</sup> I. Terasaki, *Physica B* **328**, 63 (2003)
- <sup>4</sup> Y. Wang, N. S. Rogado, R. J. Cava and N. P. Ong, *Nature* **423**, 425 (2003)
- <sup>5</sup> K. Takada, H. Sakurai, E. Takayama-Muromachi, F. Izumi, R. A. Dilanian, and T. Sasaki, *Nature* **422**, 53 (2003)
- <sup>6</sup> C. A. Marianetti, G. Kotliar, and G. Ceder, *Phys. Rev. Lett.* **92**, 196405 (2004)
- <sup>7</sup> M. D. Johannes and D. J. Singh, *Phys. Rev. B* **70**, 14507 (2004)
- <sup>8</sup> M. L. Foo, Y. Wang, S. Watauchi, H. W. Zandbergen, T. He, R. J. Cava, and N. P. Ong, *Phys. Rev. Lett.* **92**, 247001 (2004)
- <sup>9</sup> D. J. Singh, *Phys. Rev. B* **61**, 13397 (2000)
- <sup>10</sup> D. J. Singh, *Phys. Rev. B* **68**, 020503(R) (2003)
- <sup>11</sup> J. Ni and G.-M. Zhang, *Phys. Rev. B* **69**, 214503 (2004).
- <sup>12</sup> V. I. Anisimov, F. Aryasetiawan and A. I. Lichtenstein, *J. Phys.: Condens. Matter* **9** 767 (1997).
- <sup>13</sup> L.-J. Zou, J.-L. Wang and Z. Zeng, *Phys. Rev. B* **69**, 132505 (2004).
- <sup>14</sup> J. Kunes, K.-W. Lee, and W. E. Pickett, arXiv:cond-mat/0308388.
- <sup>15</sup> K.-W. Lee, J. Kunes, and W. E. Pickett, *Phys. Rev. B* **70**, 45104 (2004)
- <sup>16</sup> Q. Huang, M. L. Foo, J. W. Lynn, H. W. Zandbergen, G. Lawes, Y. Wang, B. H. Toby, A. P. Ramirez, N. P. Ong, R. J. Cava, arXiv:cond-mat/0402255.
- <sup>17</sup> H. W. Zandbergen, M. L. Foo, Q. Xu, V. Kumar, R. J. Cava, arXiv:cond-mat/0403206.
- <sup>18</sup> G. Kresse and J. Furthmuller, *Comput. Mater. Sci.* **6**, 15 (1996)
- <sup>19</sup> G. Kresse and J. Furthmuller, *Phys. Rev. B* **54**, 11169 (1996).
- <sup>20</sup> J. P. Perdew, J. A. Chevary, S. H. Vosko, Koblar A. Jackson, Mark R. Pederson, D. J. Singh, and C. Fiolhais, *Phys. Rev. B* **46**, 6671 (1992).
- <sup>21</sup> S. H. Vosko, L. Wilk and M. Nusair, *Can. J. Phys.* **58**, 1200 (1980)
- <sup>22</sup> P. E. Blochl, *Phys. Rev. B* **50**, 17953 (1994)
- <sup>23</sup> G. Kresse and D. Joubert, *Phys. Rev. B* **59**, 1758 (1996)

- <sup>24</sup> H. J. Monkhorst and J. D. Pack, Phys. Rev. B **13**, 5188 (1976).
- <sup>25</sup> P. E. Blochl, O. Jepsen, and O. K. Andersen, Phys. Rev. B **49**, 16223 (1994)
- <sup>26</sup> S. L. Dudarev, G. A. Botton, S. Y. Savrasov, C. J. Humphreys, A. P. Sutton, Phys. Rev. B **57**, 1505 (1998)
- <sup>27</sup> A. Kokalj, J. Mol. Graphics Mod. **17**, 176 (1999). Code available from <http://www.xcrysden.org/>.
- <sup>28</sup> M. Coey, Nature, 430, 155 (2004)
- <sup>29</sup> M. A. Korotin, S. Yu. Ezhov, I. V. Solovyev, V. I. Anisimov, D. I. Khomskii and G. A. Sawatzky, Phys. Rev. B **54**, 5309 (1996)
- <sup>30</sup> H. Sakurai, K. Takada, S. Yoshii, T. Sasaki, K. Kindo, and E. Takayama-Muromachi, Phys. Rev. B **68**, 132507 (2003)
- <sup>31</sup> T. Fujimoto, G.-Q. Zheng, Y. Kitaoka, R. L. Meng, J. Cmaidalka, and C. W. Chu, Phys. Rev. Lett. **92**, 047004 (2003)
- <sup>32</sup> A. Chainani, T. Yokoya, Y. Takata, K. Tamasaku, M. Taguchi, T. Shimojima, N. Kamakura, K. Horiba, S. Tsuda, S. Shin, D. Miwa, Y. Nishino, T. Ishikawa, M. Yabashi, K. Kobayashi, H. Namatame, M. Taniguchi, K. Takada, T. Sasaki, H. Sakurai, E. Takayama-Muromachi, arXiv:cond-mat/0312293.
- <sup>33</sup> F. C. Chou, J. H. Cho, P. A. Lee, E.T. Abel, K. Matan, and Y. S. Lee, arXiv:cond-mat/0306659.
- <sup>34</sup> A. T. Boothroyd, R. Coldea, D. A. Tennant, D. Prabhakaran, L. M. Helme, and C. D. Frost, Phys. Rev. Lett. **92**, 197201 (2004)
- <sup>35</sup> T. Motohashi, R. Ueda, E. Naujalis, T. Tojo, I. Terasaki, T. Atake, M. Karppinen, and H. Yamauchi, Phys. Rev. B **67**, 64406 (2003)

FIG. 1: (Color online) The optimized crystal structure of  $\text{Na}_{0.5}\text{CoO}_2$ . The designations of the Na and Co atoms are as indicated.

FIG. 2: GGA paramagnetic band structure (left panel) and density of states (DOS)(right panel) of  $\text{Na}_{0.5}\text{CoO}_2$ . The Fermi energy is at zero.  $\Gamma=(0,0,0)$ ,  $M=(1/2,0,0)$ ,  $N=(1/2,1/2,0)$ , and  $A=(0,0,1/2)$ . The dot line in the DOS panel represents the Co  $a_g$  partial DOS.

FIG. 3: (Color online) (a) Schematic diagram of the reciprocal lattice and the first Brillouin zone for the original  $P6_3/mmc$  lattice (black) and the superstructure adopted in this work (red) respectively. (b)-(f) Top views of Fermi surface within the first Brillouin zone for band 96 to band 100 of  $\text{Na}_{0.5}\text{CoO}_2$  respectively.

FIG. 4: (Color online) Density of states (DOS) for FM phase. Total DOS, O  $2p$  partial DOS, and  $3d$  partial DOS of Co1 and Co2 for (a) GGA result and  $U =$  (b) 3.0, (c) 4.0, and (d) 7.0 eV are presented.

FIG. 5: (Color online) Density of states (DOS) for AFM1 phase. Total DOS, O  $2p$  partial DOS, and  $3d$  partial DOS of Co1 and Co2 for (a) GGA result and  $U =$  (b) 3.0, (c) 4.0, and (d) 7.0 eV are presented.

FIG. 6: (Color online) Density of states (DOS) for AFM2 phase. Total DOS, O  $2p$  partial DOS, and  $3d$  partial DOS of Co1 and Co2 for (a) GGA result and  $U =$  (b) 3.0, (c) 4.0, and (d) 7.0 eV are presented.

FIG. 7: (Color online) Effect of the intra-atomic repulsion  $U$  on (a) magnetic moments, (b) energy gap and (c) energy difference between AFM and FM states of  $\text{Na}_{0.5}\text{CoO}_2$ . The energy of FM state is set to zero.

TABLE I: Optimized structural parameters. Experimental values are presented in parentheses.

Atom	Site	x	y	z
Co1	$4f$	0.003 (0)	0.250 (1/4)	0.003 (0)
Co2	$4d$	0.500 (1/2)	0.000 (0)	0.000 (0)
Na1	$2b$	-0.030 (-0.018)	0.250 (1/4)	0.750 (3/4)
Na2	$2a$	0.355 (0.352)	0.750 (3/4)	0.750 (3/4)
O1	$4f$	0.336 (1/3)	0.250 (1/4)	0.0880 (0.0895)
O2	$4f$	0.330 (1/3)	0.750 (3/4)	0.0845 (0.0820)
O3	$8g$	-0.166 (1/6)	0.000 (0)	0.0892 (0.0895)

Figure 1, Li *et al.*

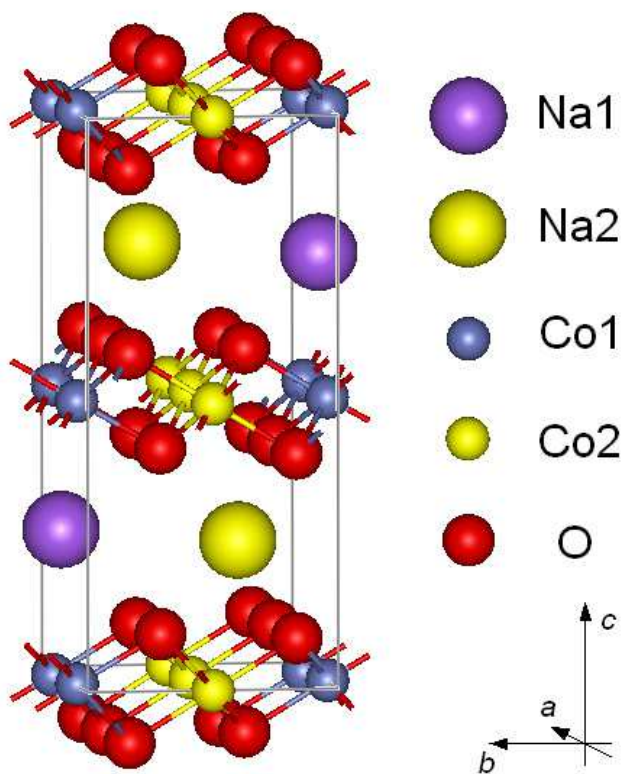


Figure 2, Li *et al.*

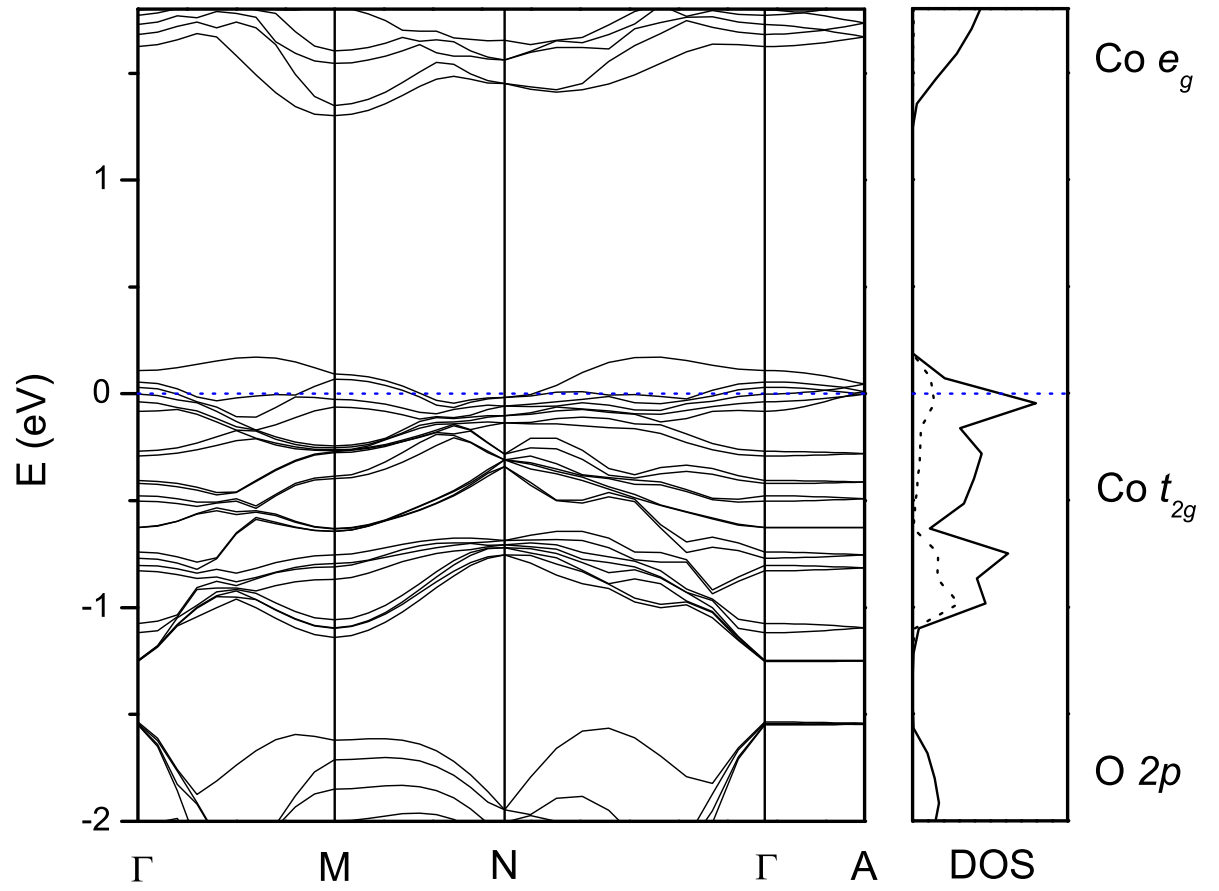




Figure 3, Li *et al.*

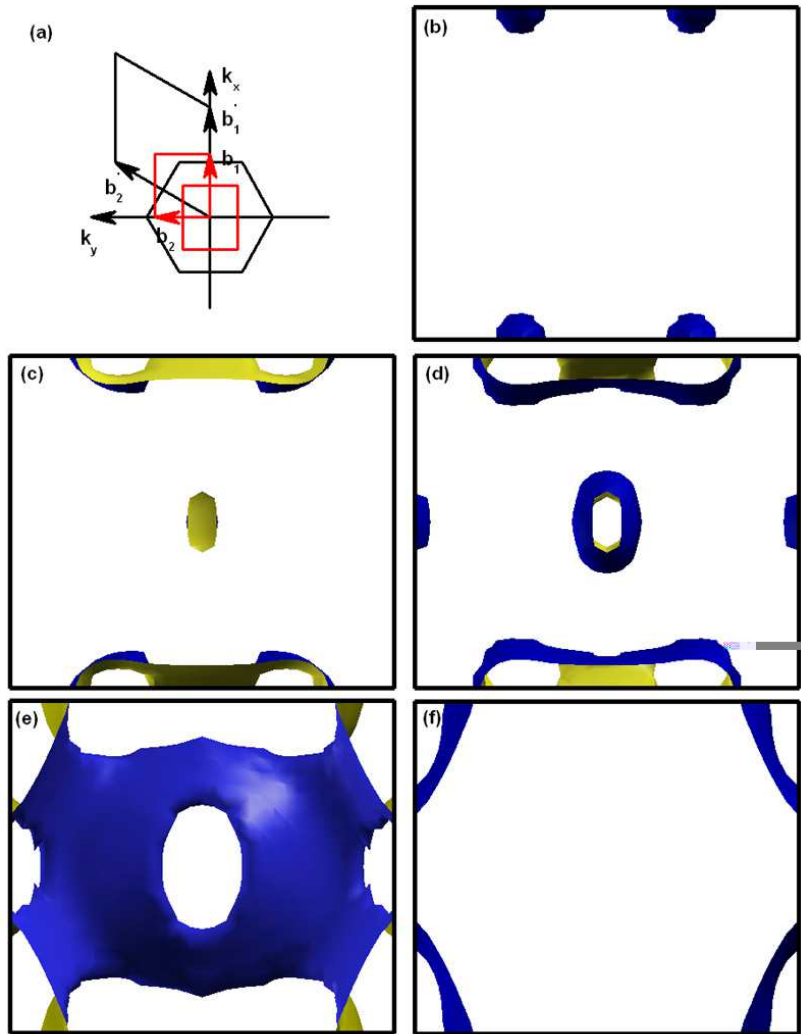


Figure 4, Li *et al.*

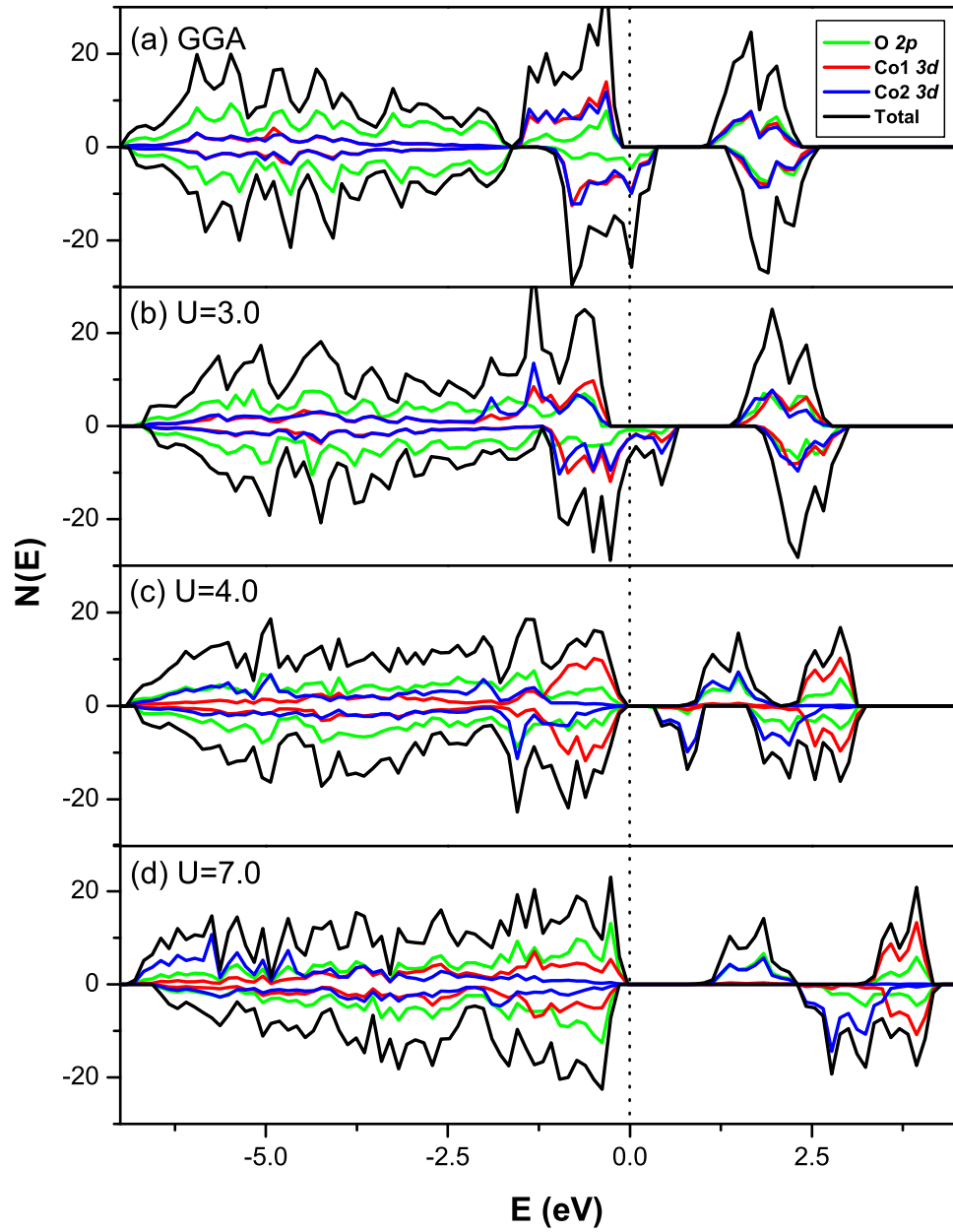


Figure 5, Li *et al.*

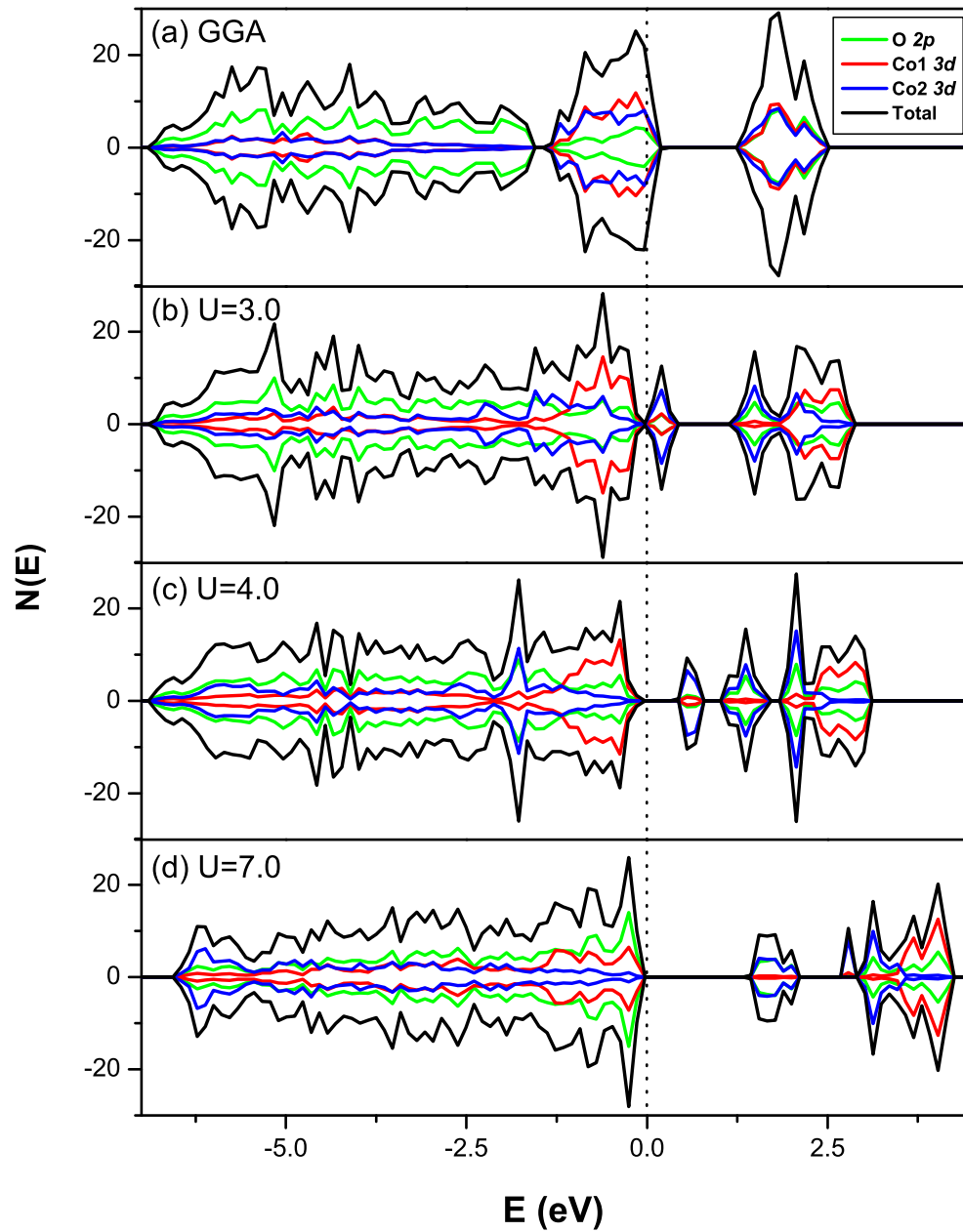


Figure 6, Li *et al.*

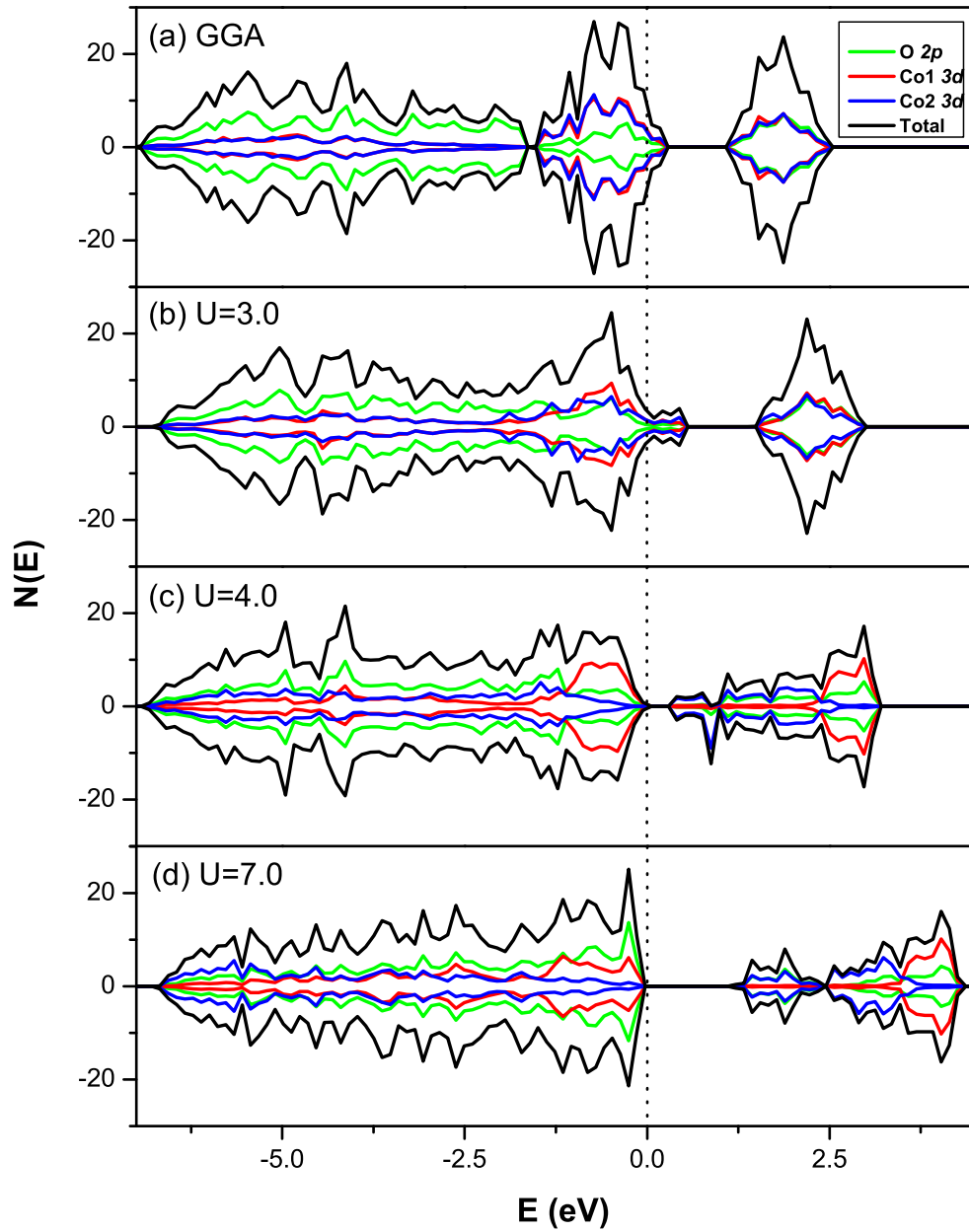


Figure 7, Li *et al.*

